August 23, 2001

Measurement of dijet cross-sections at low Q^2 at HERA

H1 Collaboration

Abstract

Triple differential dijet cross-sections in $e^{\pm}p$ interactions measured with the H1 detector at HERA are presented in the region of photon virtuality $2\ \mathrm{GeV}^2 < Q^2 < 80\ \mathrm{GeV}^2$, inelasticity $0.1 < y < 0.85$, low transverse jet momentum $E_t^{jet\,1,2} > 5\ \mathrm{GeV}$, $\overline{E}_t > 6\ \mathrm{GeV}$, and pseudorapidity $-2.5 < \eta^{*\,jet\,1,2} < 0$. The data are compared to Monte Carlo simulations which differ in their assumptions about photon structure and employ DGLAP or CCFM parton evolution scheme. Indications of effects connected with the resolved processes of longitudinally polarized virtual photons are investigated for the first time.

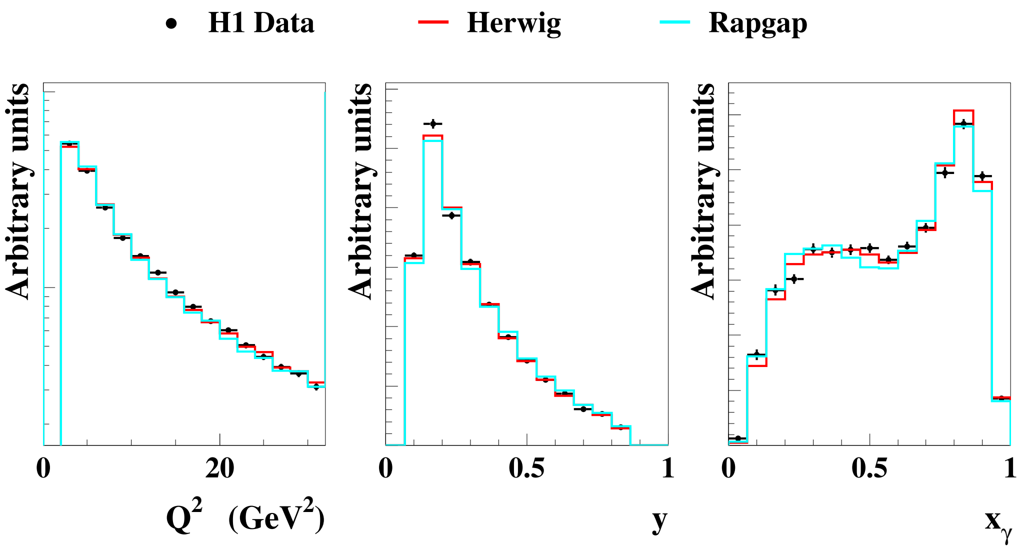

Figure 1: Detector level comparison of the data with HERWIG and RAPGAP simulations. Both HERWIG and RAPGAP are reweighted to describe the data. All detector level selection criteria were applied.

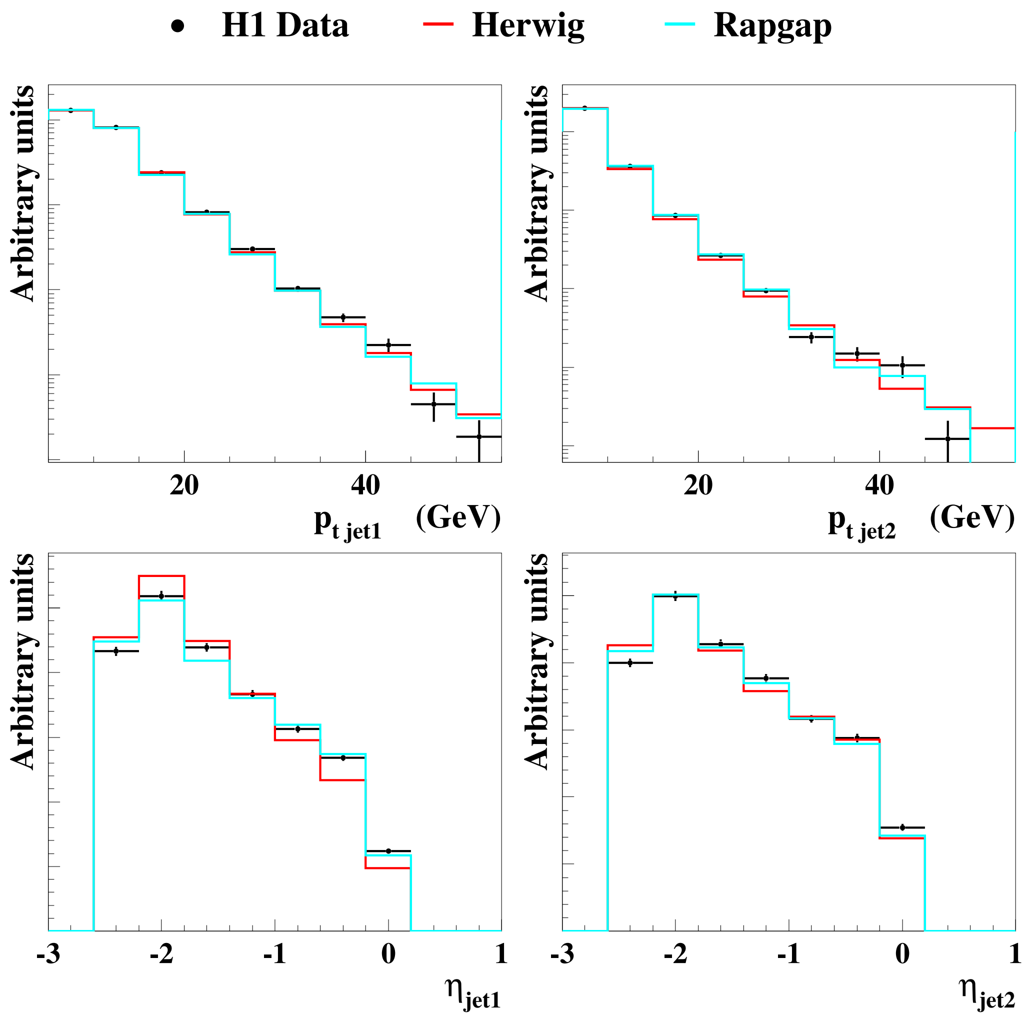

Figure 2: Detector level comparison of the data with HERWIG and RAPGAP simulations. Both HERWIG and RAPGAP are reweighted to describe the data. All detector level selection criteria were applied.

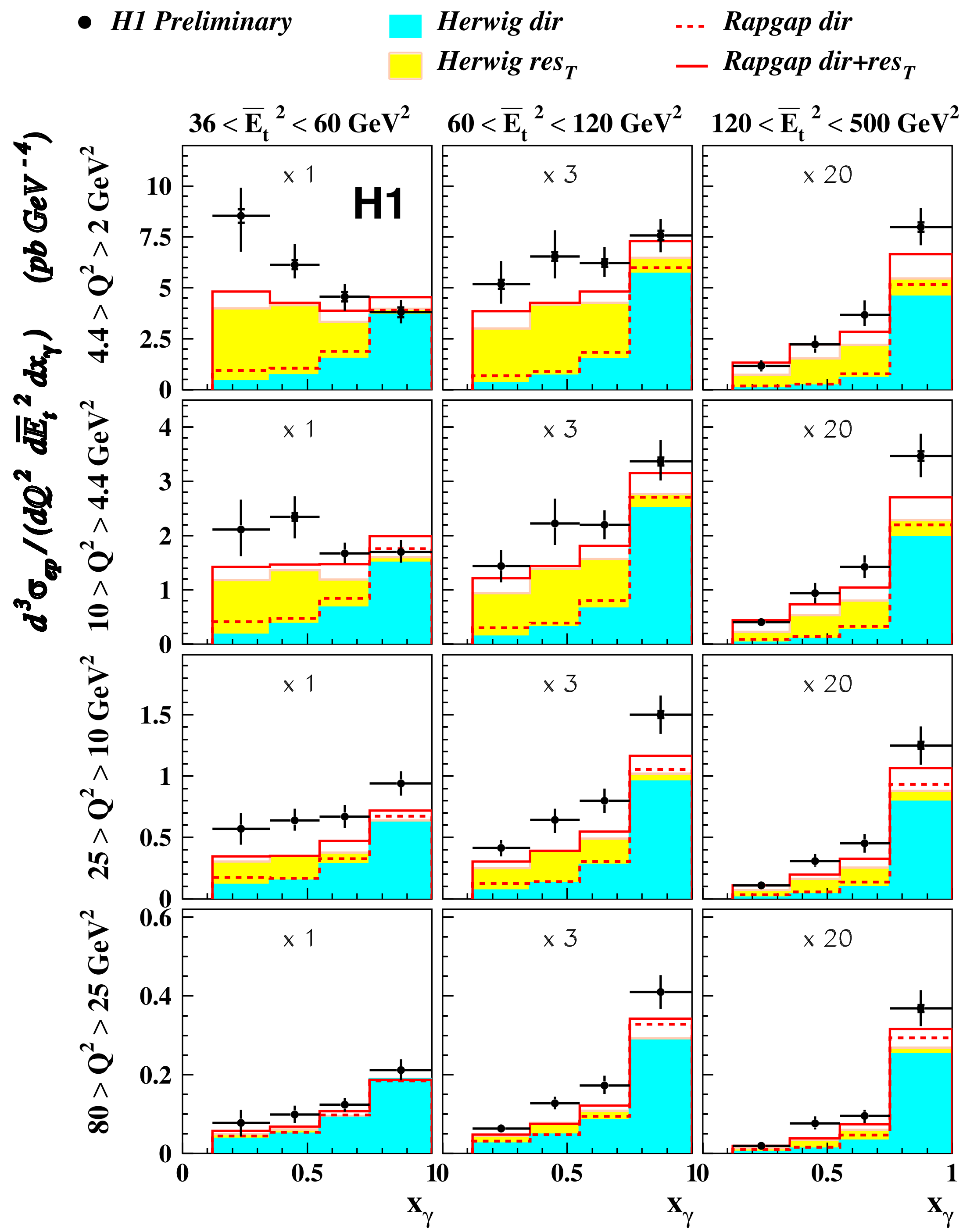

Figure 3: Triple differential dijet cross-section as a function of x_γ , $\overline{E}_t^2$ and Q^2. The data are compared to HERWIG and RAPGAP MC predictions. Separately shown are the direct (dir) and the resolved component of transversally polarized γ (res$_T$).

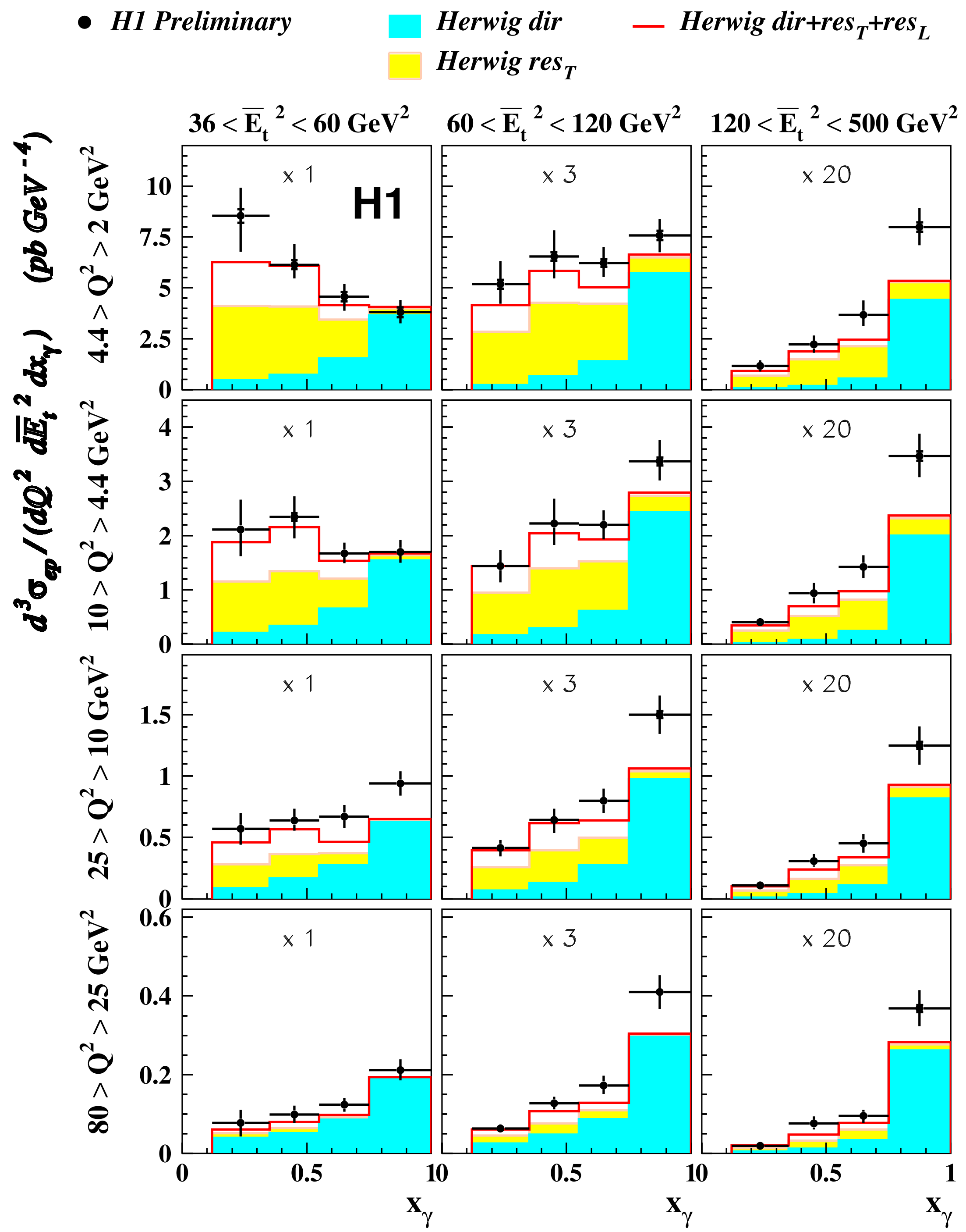

Figure 4: Triple differential dijet cross-section as a function of x_γ , $\overline{E}_t^2$ and Q^2. The data are compared to HERWIG with an additional contribution of the longitudinally polarized photon processes (res$_L$).

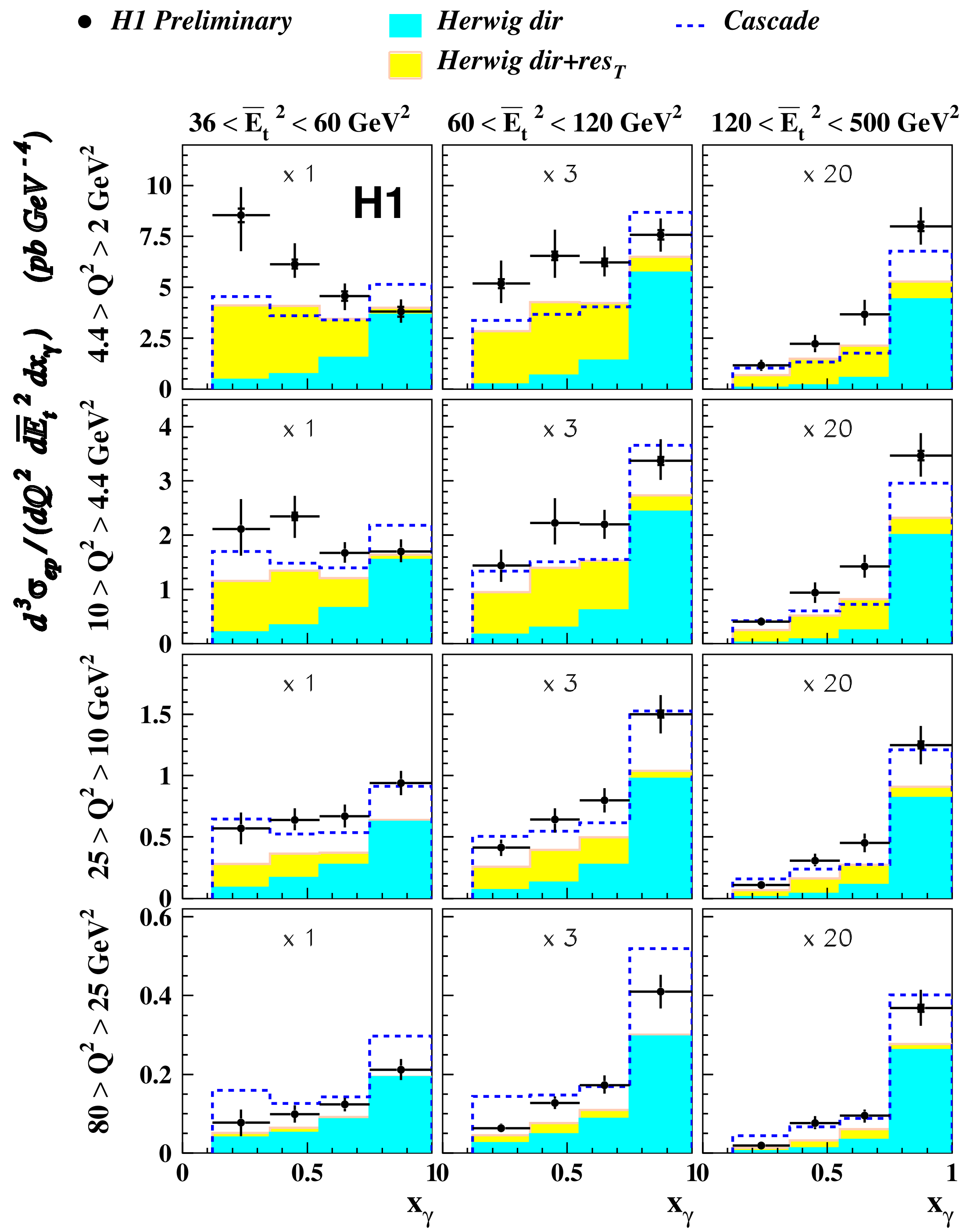

Figure 5: Triple differential dijet cross-section as a function of x_γ , $\overline{E}_t^2$ and Q^2. The data are compared to HERWIG and CASCADE MC, which is based on the CCFM evolution scheme.

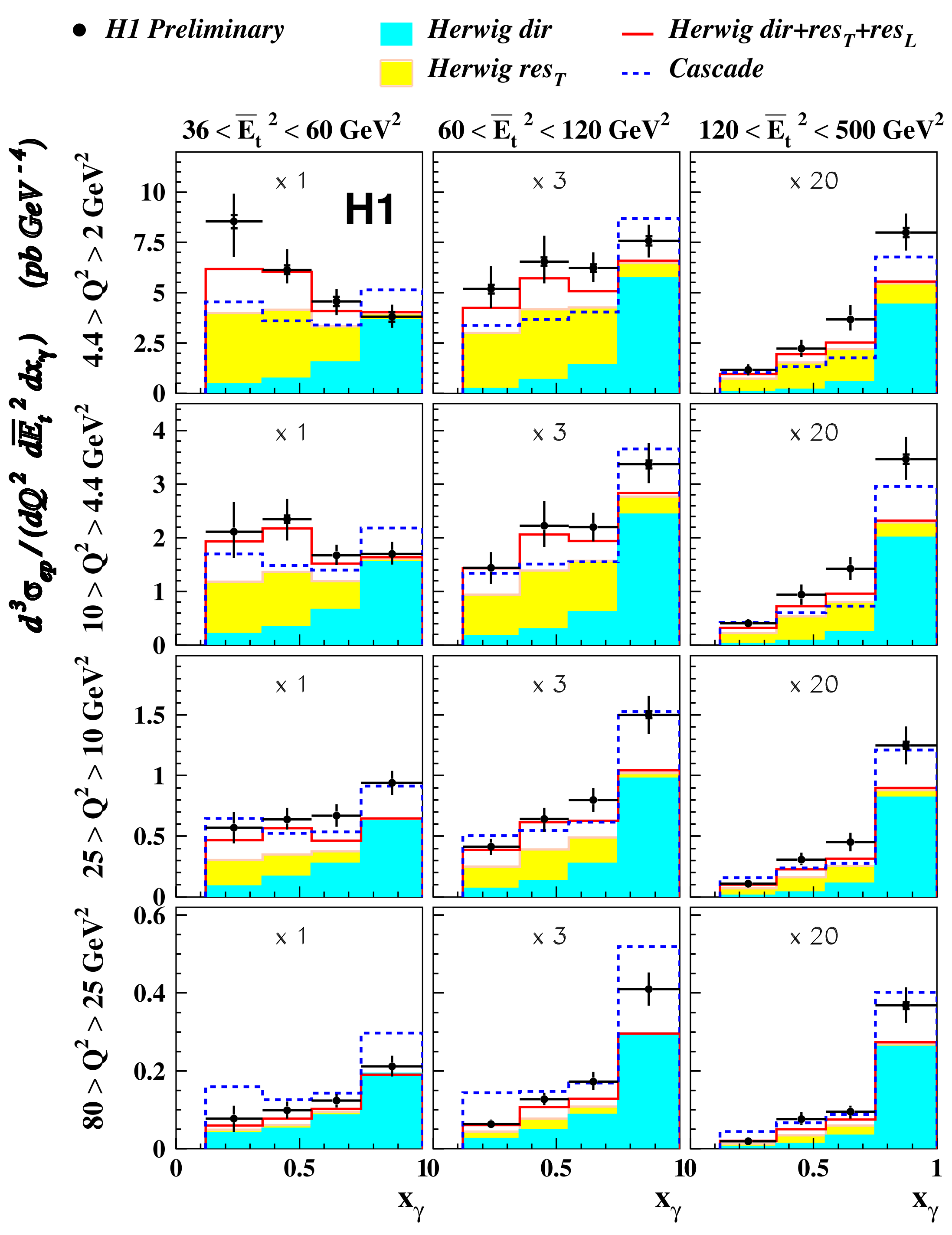

Figure 6: Triple differential dijet cross-section as a function of y, x_γ and Q^2. Combination of Figure 4 and 5 is plotted here.

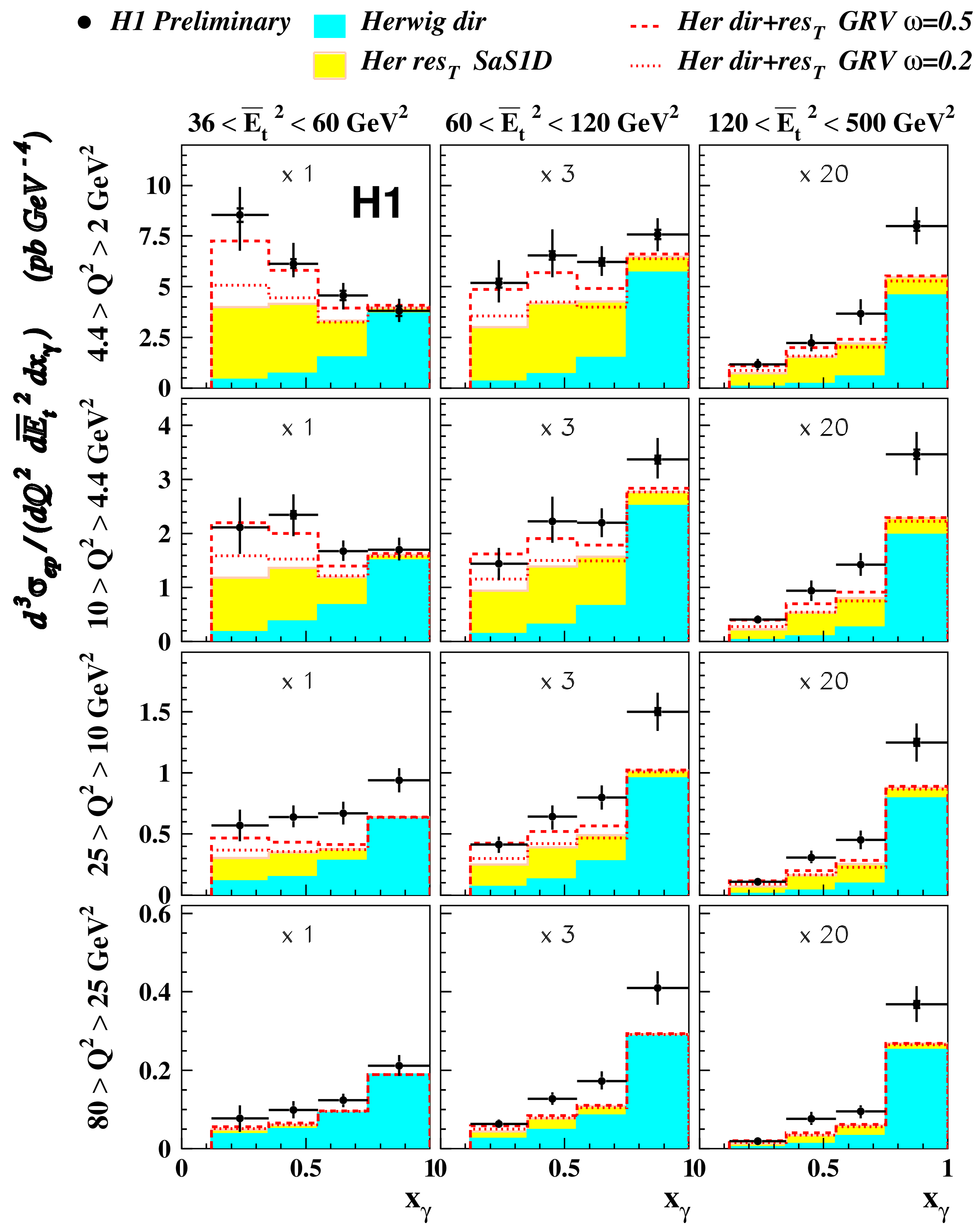

Figure 7: Triple differential dijet cross-section as a function of y, x_γ and Q^2. The data are compared to HERWIG with different γ_T^* PDFs. ω is a parameter from the Drees-Godbole factor, which suppresses the GRV γ PDFs with Q^2.

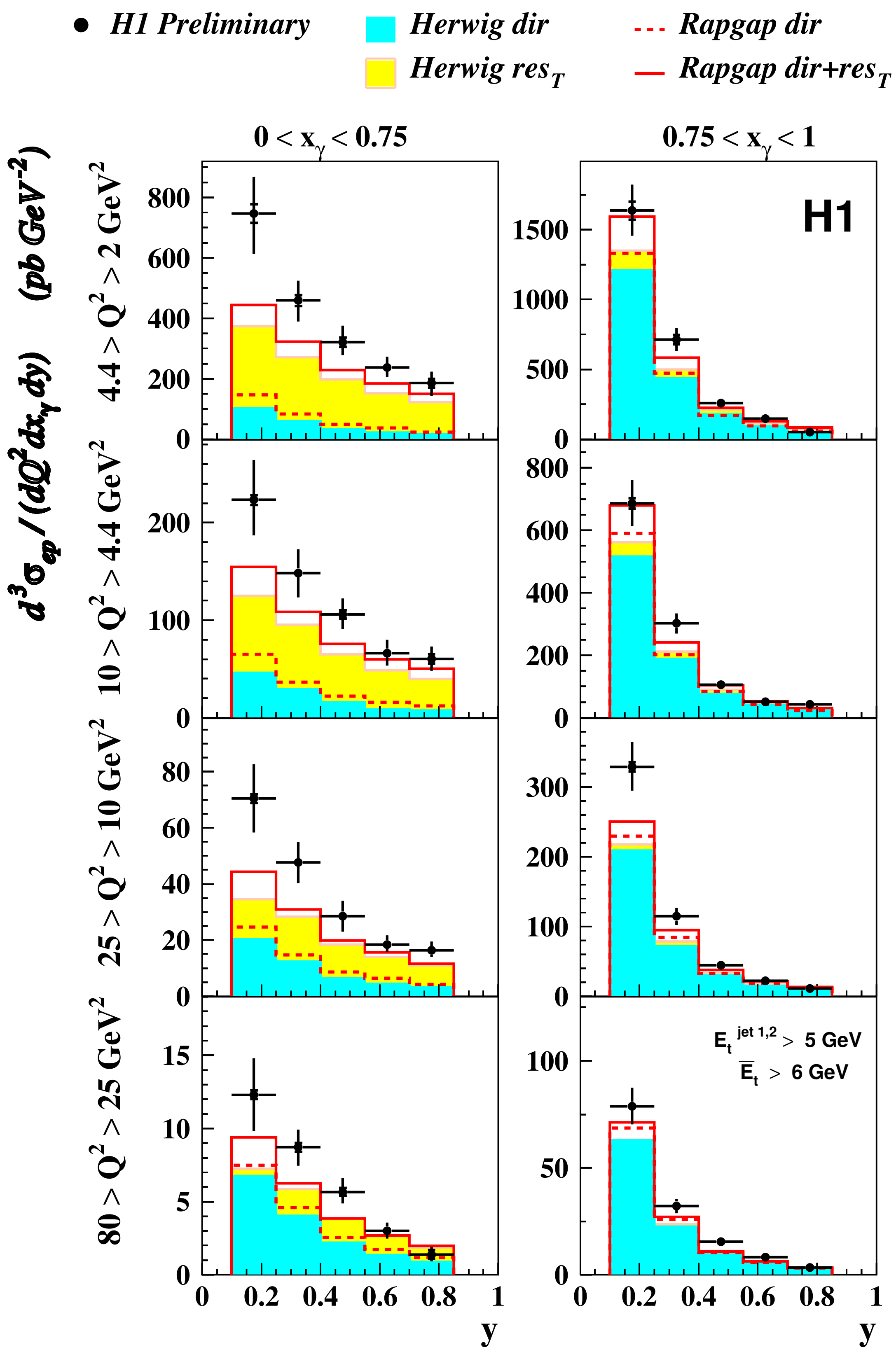

Figure 8: Triple differential dijet cross-section as a function of y, x_γ and Q^2. The data are compared to HERWIG and RAPGAP MC predictions. Both MC models underestimate the data, especially in low x_γ and low y range.

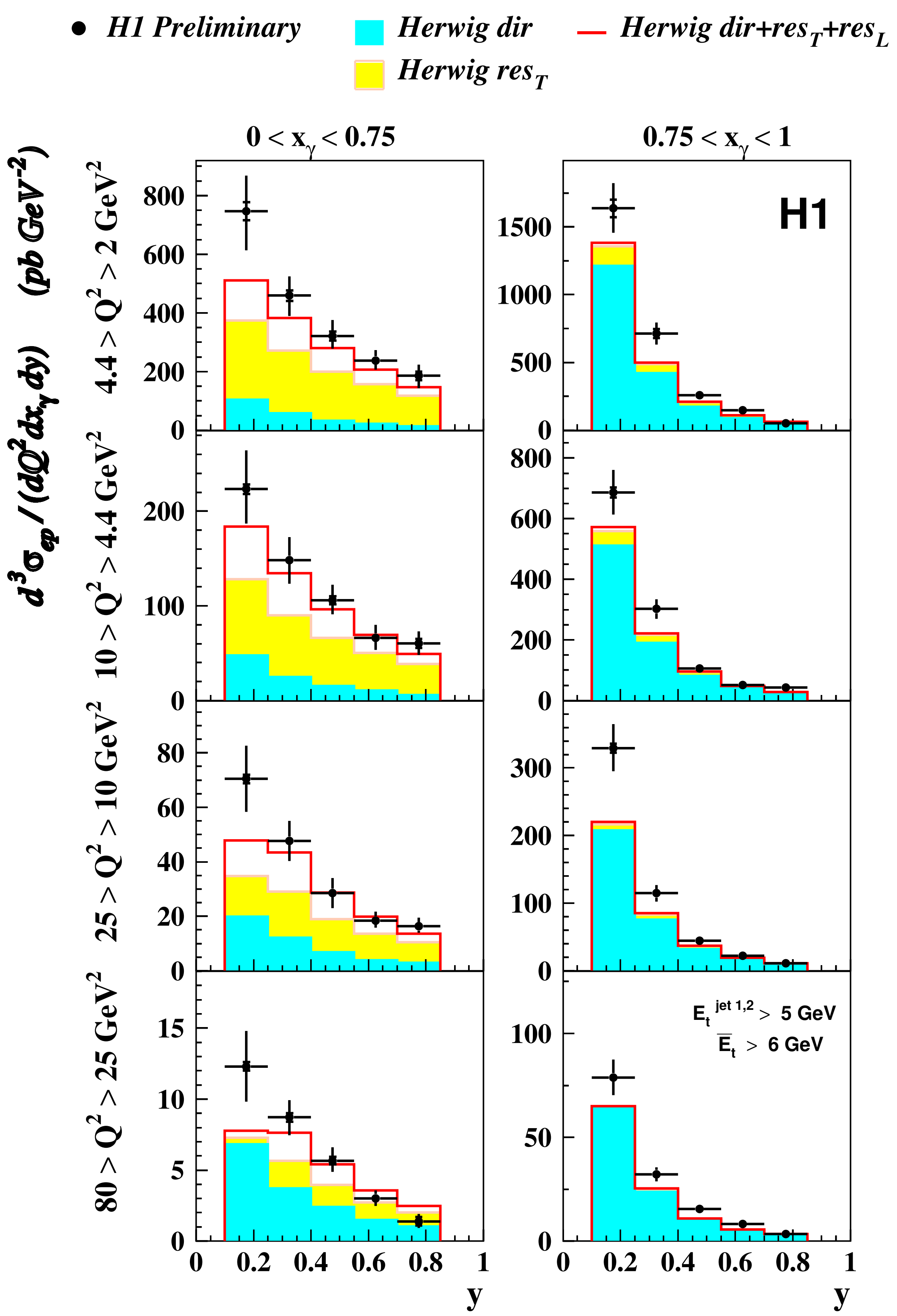

Figure 9: Triple differential dijet cross-section as a function of y, x_γ and Q^2. The data are compared to HERWIG with an additional contribution of the longitudinally polarized photon resolved processes. The additional longitudinal photon contributions lead to a better description of the slope of the y distribution.

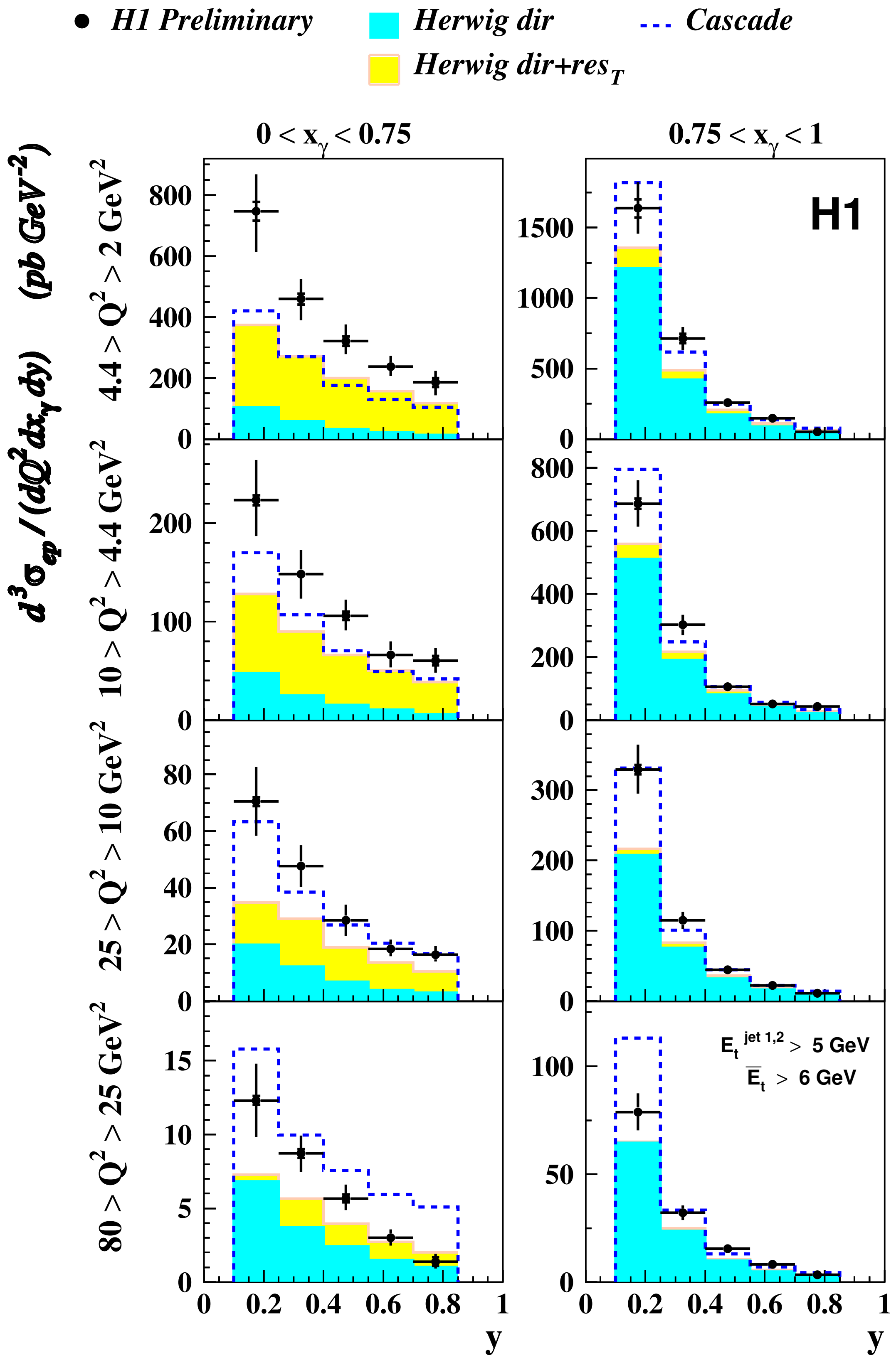

Figure 10: Triple differential dijet cross-section as a function of y, x_γ and Q^2. The data are compared to HERWIG and CASCADE MC.

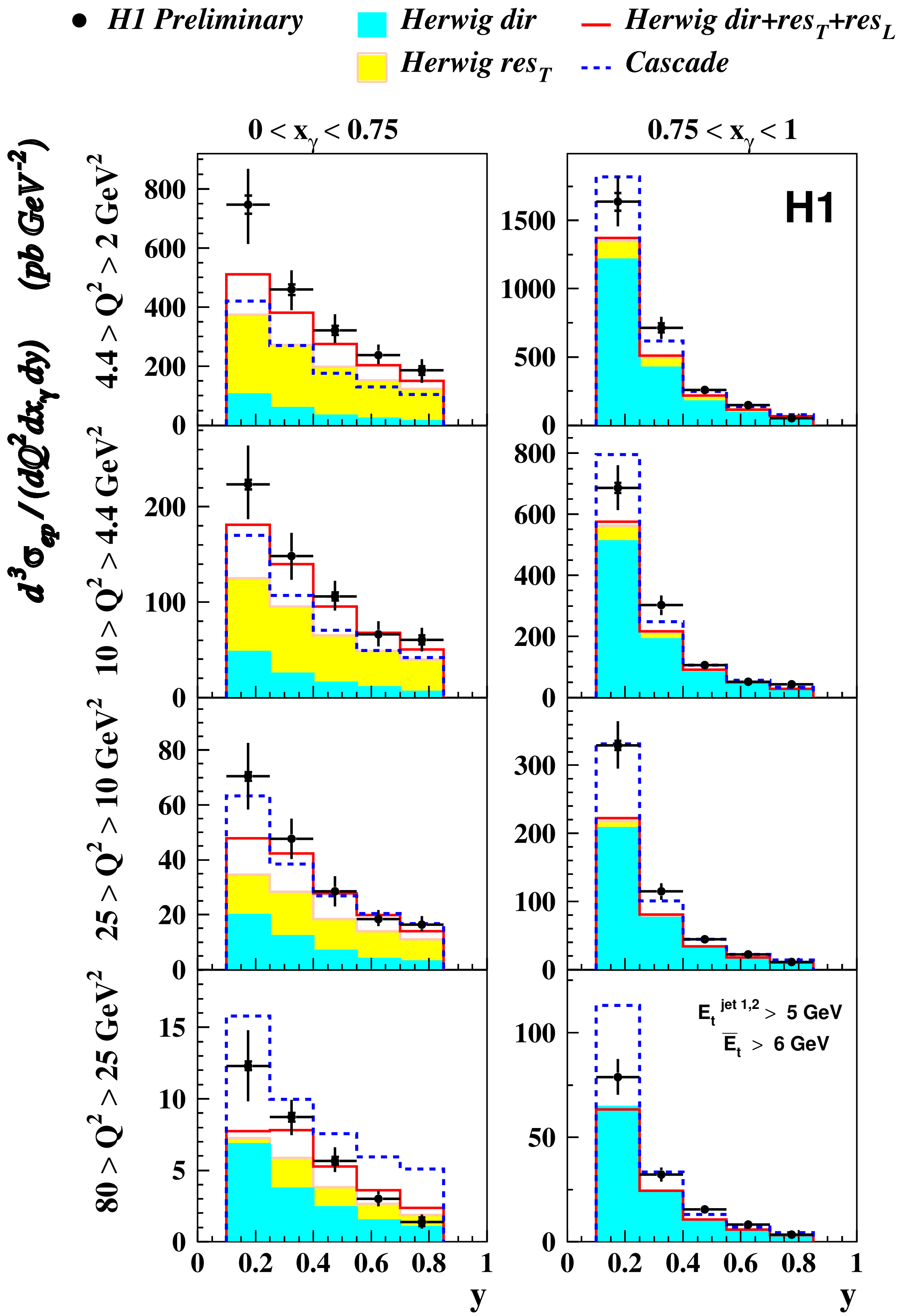

Figure 11: Triple differential dijet cross-section as a function of y, x_γ and Q^2. Combination of Figure 9 and 10 is plotted here.

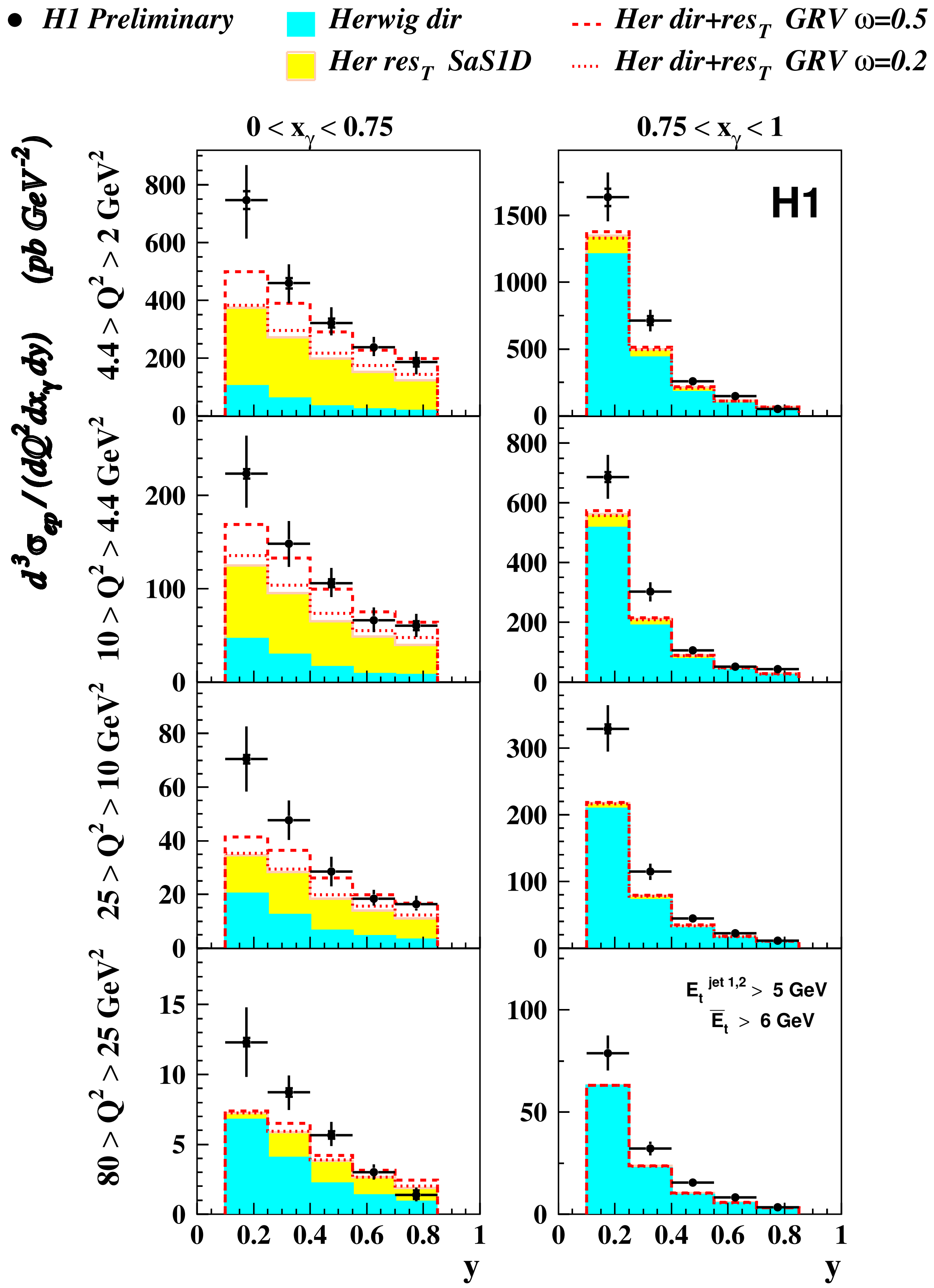

Figure 12: Triple differential dijet cross-section as a function of y, x_γ and Q^2. The data are compared to HERWIG with different γ_T^* PDFs. The slope of y distributions are steeper in the data than in any of the HERWIG predictions plotted.

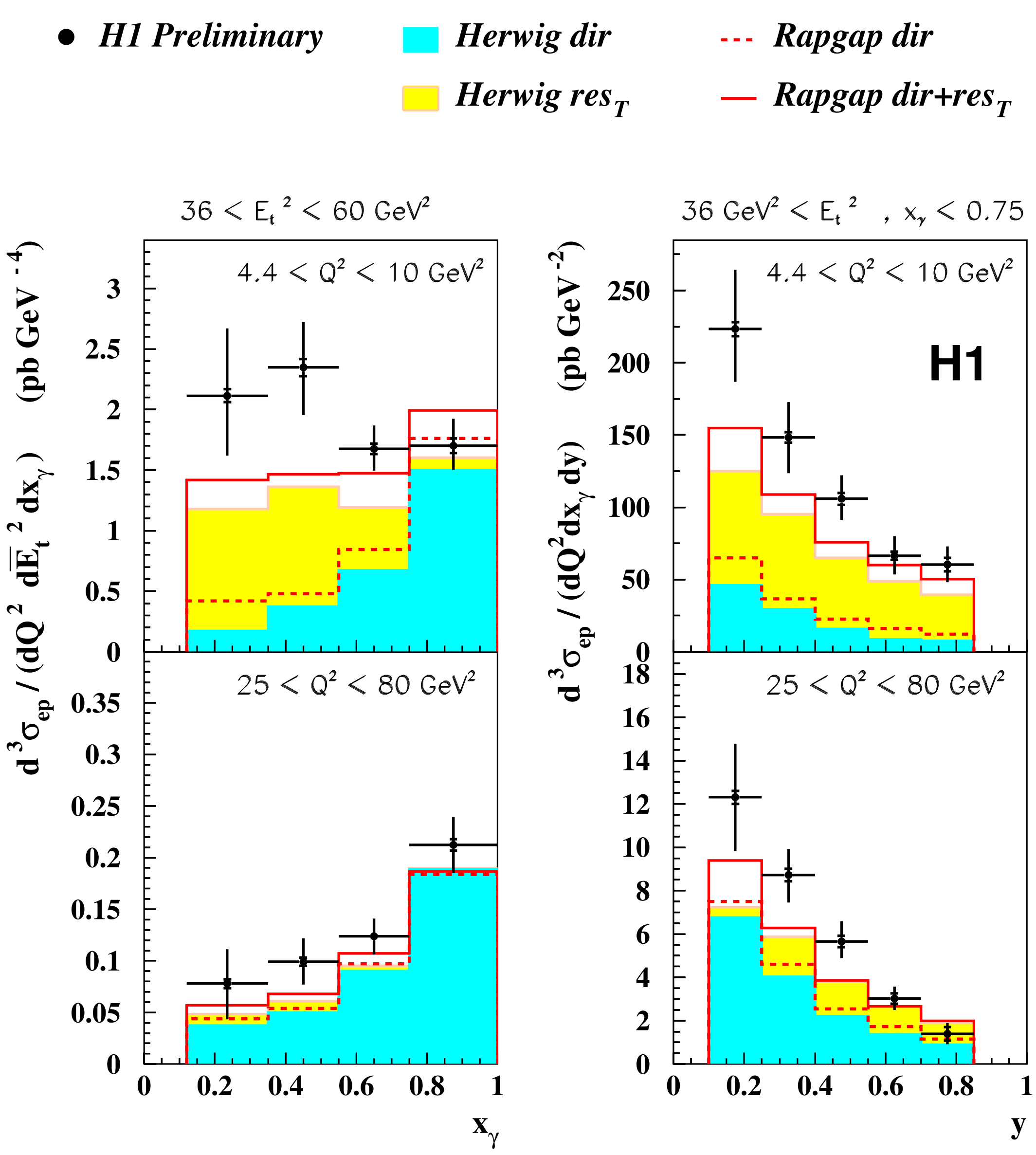

Figure 13: Simplified version of Fig. 3 and 8

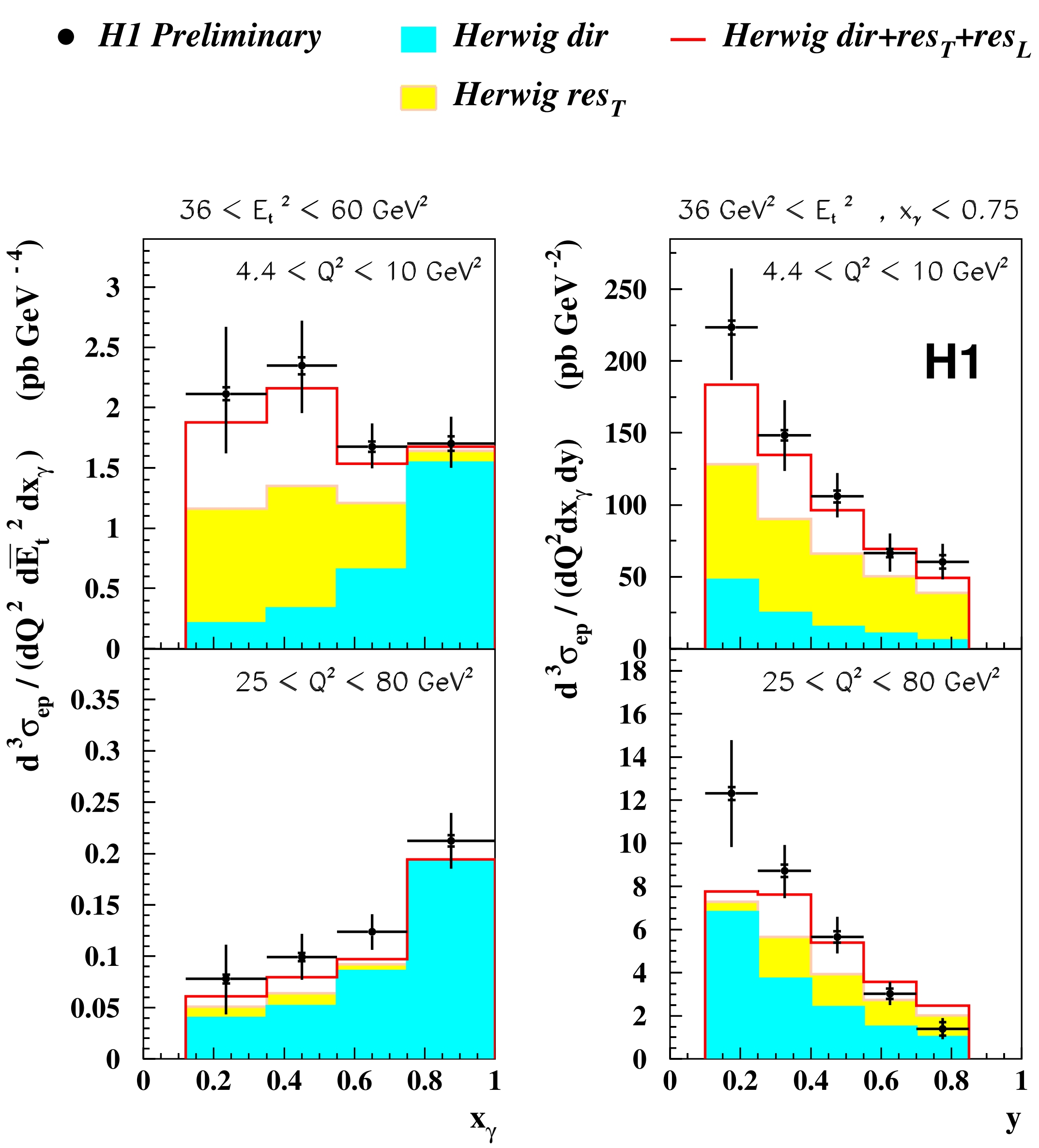

Figure 14: Simplified version of Fig. 4 and 9

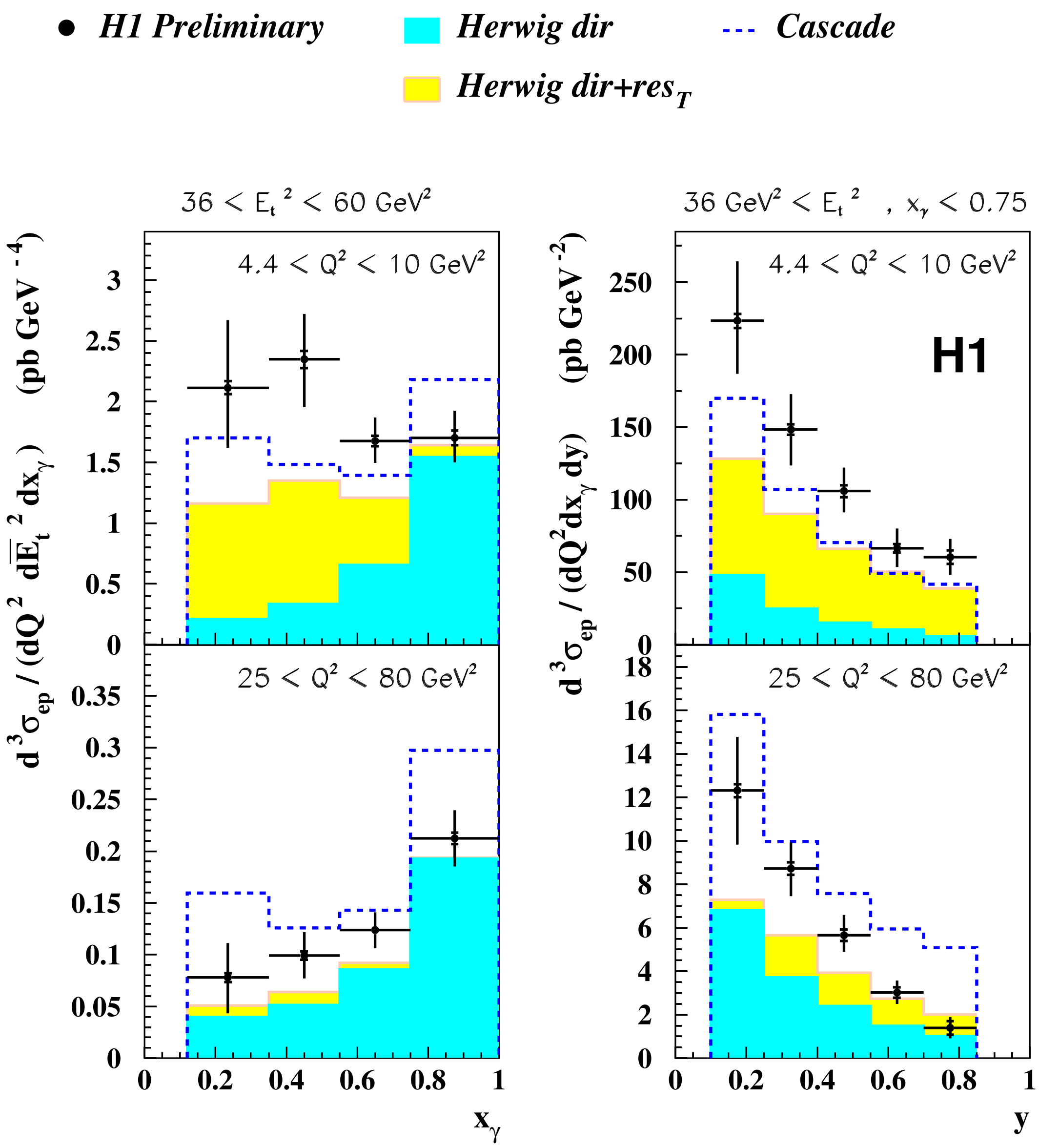

Figure 15: Simplified version of Fig. 5 and 10

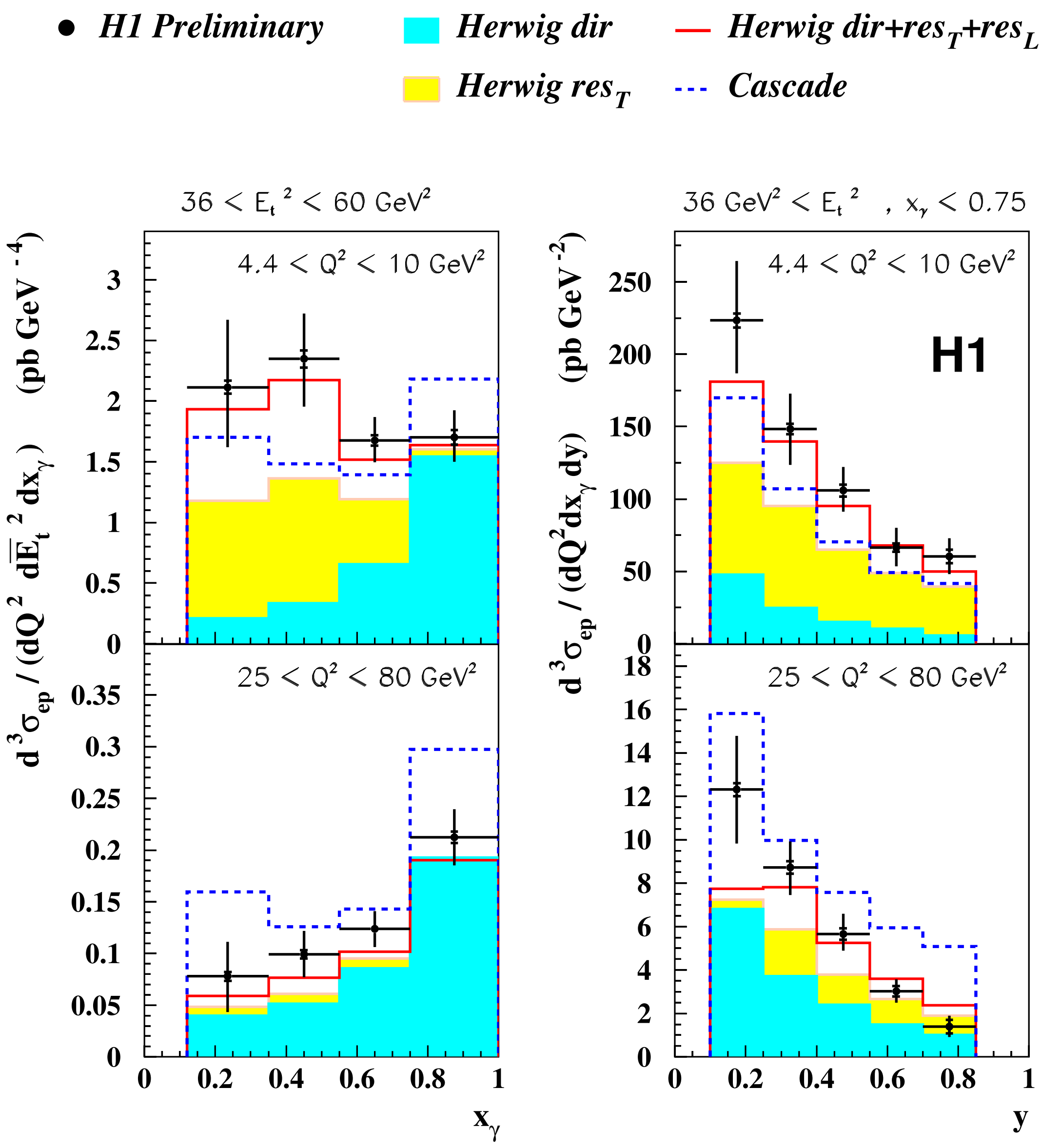

Figure 16: Simplified version of Fig. 6 and 11

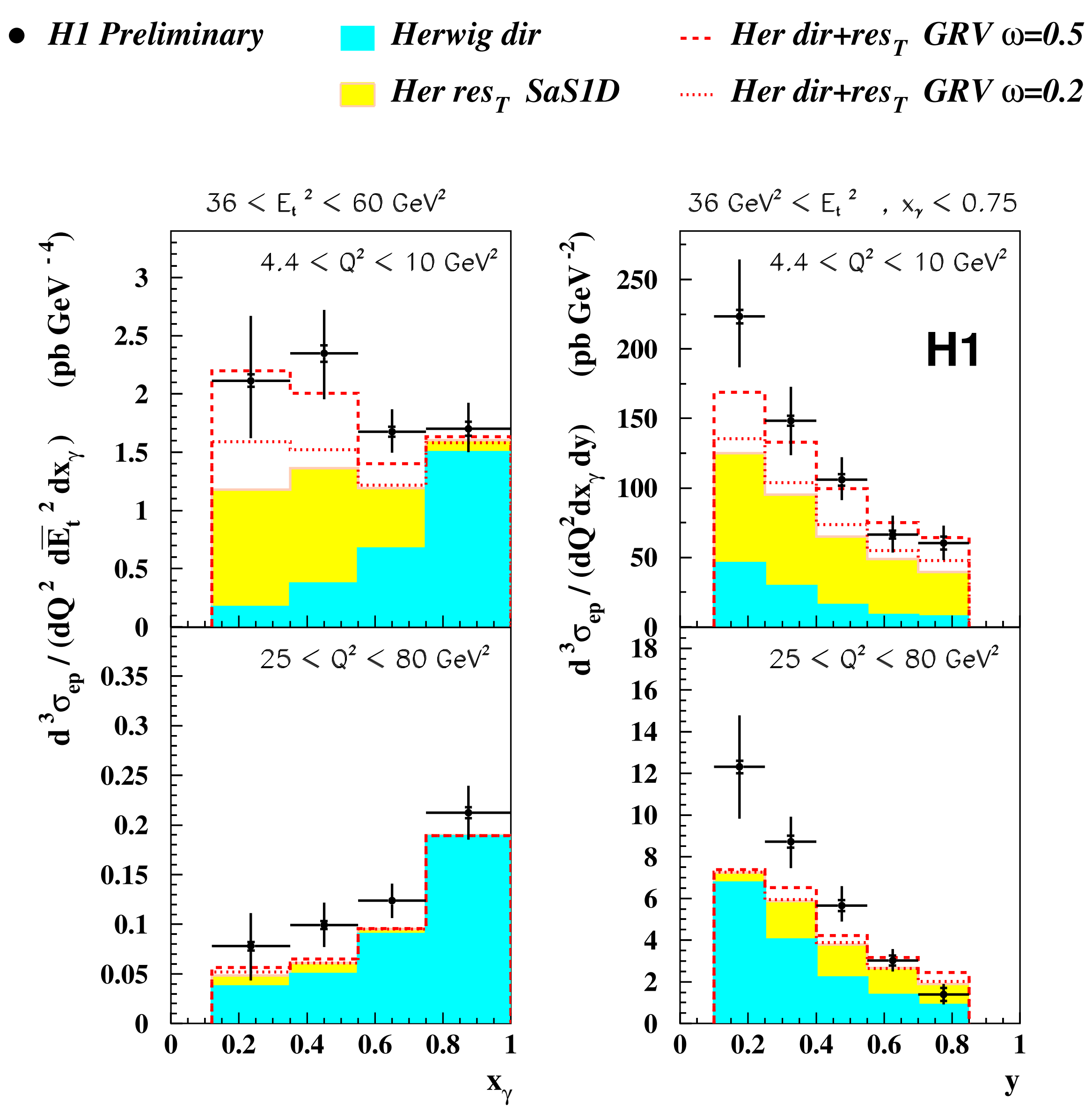

Figure 17: Simplified version of Fig. 7 and 12